

# Detection of X-Ray Emission from the Unidentified TeV Gamma-Ray Source TeV J2032+4130

Hiroshi MURAKAMI, Shunji KITAMOTO

*Department of Physics, Rikkyo University, 3-34-1 Nishi-Ikebukuro, Toshima-ku, Tokyo 171-8501*

*hiro@rikkyo.ac.jp*

Akiko KAWACHI

*Department of Physics, Tokai University, Kitakaname 1117, Hiratsuka, Kanagawa 259-1292*

and

Takeshi NAKAMORI

*Research Institute for Science and Engineering, Waseda University, 3-4-1 Okubo, Shinjuku-ku, Tokyo 169-8555*

(Received 2011 June 14; accepted 2011 July 29)

## Abstract

We observed the first unidentified TeV  $\gamma$ -ray source TeV J2032+4130 with Suzaku. Owing to Suzaku's high sensitivity for detection of diffuse X-ray emission, we found two small structures in the TeV emitting region. One of them is coincident with a  $\gamma$ -ray pulsar PSR J2032+4127, which was discovered by the Fermi Gamma-ray Space Telescope. By subtracting contribution of point sources estimated by Chandra data, we obtained diffuse X-ray spectrum. The X-ray spectrum can be reproduced by a power-law model with a photon index of  $\sim 2$ , and an X-ray flux of  $2 \times 10^{-13}$  erg s $^{-1}$  cm $^{-2}$ . The ratio of the  $\gamma$ -ray flux to the X-ray flux is about 10. If the origin of the TeV  $\gamma$ -ray is inverse Compton scattering of microwave background by high energy electrons, the ratio corresponds to the magnetic field strength of  $\sim 1$   $\mu$ G. However, the smaller size of the X-ray emission than that of the TeV emission suggests that energy loss of the electrons can explain the large ratio of the  $\gamma$ -ray flux with a reasonable magnetic field strength of a few  $\mu$ G.

**Key words:** acceleration of particles — X-rays: individual (TeV J2032+4130) — X-rays: ISM — pulsars: individual (PSR J2032+4127)

## 1. Introduction

The stereoscopic technique of atmospheric Cerenkov telescopes improved the angular resolution for detecting TeV  $\gamma$ -rays and thus increased the number of TeV  $\gamma$ -ray sources. Some of new TeV objects have no counterparts at other wavelengths and are called unidentified TeV  $\gamma$ -ray objects. These objects provide key information in the investigation of the origin of high-energy cosmic rays. Multi-wavelength observations of these objects are very important in elucidating the emission mechanism and successful identification of them.

TeV J2032+4130 was the first unidentified TeV  $\gamma$ -ray source discovered by HEGRA (Aharonian et al. 2002). The TeV emission exhibits a significant extension with a radius of 6'.2 and a center of gravity of (R.A., Dec) = (20<sup>h</sup>31<sup>m</sup>57<sup>s</sup>.0, 41°29'56"8) (Aharonian et al. 2005a). The position is coincident with an OB association, Cyg OB2, and located in north of a microquasar, Cyg X-3. These two sources had been suggested to be possible origins of TeV  $\gamma$ -rays, but no firm evidence to determine the counterpart has been found. TeV  $\gamma$ -ray emission of this region has also been reported by other telescopes: Whipple, MAGIC, and Milagro (Konopelko et al. 2007, Albert et al. 2008, Abdo et al. 2007).

In the X-ray band, Chandra and XMM-Newton observed the TeV J2032+4130 region. The first observation by Chandra detected 27 point sources within the observed

field ( $\sim 17'$ ) with the exposure time of 5 ks (Mukherjee et al. 2003, MHG2003 hereafter,). Butt et al. (2003) also resolve 19 point sources above the threshold of 2.5  $\sigma$  by adapting the `wavdetect` tool to the same data. Then follow-up deeper 50 ks observation remarkably increased the number of detected sources: 240 sources in almost the same field (Butt et al. 2006, But2006 hereafter).

XMM-Newton also detected many point sources in the wider FOV ( $\sim 30'$ ). By subtracting the contribution of detected point sources, Horns et al. (2007) indicates a hint of diffuse emission extending about the size of TeV emission region. However, this result may still include contribution of faint point sources which were resolved by Chandra, due to the moderate angular resolution of XMM-Newton.

The detection of a diffuse X-ray emission for the 50 ks Chandra data has been also reported by Mukherjee, Gotthelf, Halpern (2007) with the same analysis technique. However, the spectral model can not be constrained because of the low photon statistics observation by Chandra.

Recently, the Large Area Telescope on the Fermi Gamma-ray Space Telescope detected  $\gamma$ -rays from this region, with the energy from 20 MeV to 300 GeV (1FGL J2032.2+4127, Abdo et al. 2010a). In addition, this  $\gamma$ -ray source showed a pulsation with a pulse period of 143 ms (PSR J2032+4127; Abdo et al. 2009, 2010b). Subsequent observation of a radio band also detected a pulsation with the consistent position and the pulse frequency of the  $\gamma$ -

ray pulsar. The position of the pulsar is coincident with the optical point source of the number 213 in Massey & Thompson (1991) (MT91 213; Camilo et al. 2009).

These results imply that the origin of TeV  $\gamma$ -rays also relates to this  $\gamma$ -ray pulsar. Active pulsars are losing a significant part of the energy via relativistic particles, and forms pulsar wind nebulae (PWNe). PWNe emit synchrotron radiation from radio to X-ray bands. In addition, some PWNe are found to be TeV emitter (Gaensler & Slane 2006, Kargaltsev & Pavlov 2010). Thus PSR J2032+4127 is a possible candidate for the counterpart of TeV J2032+4120.

The distance to the PSR J2032+4127 is estimated to be 3.6 kpc by measuring the dispersion measure in the radio band (Camilo et al. 2009). While, the distance to the Cygnus OB2 is estimated to be 1.7 kpc by a spectroscopic observation of OB stars (Hanson 2003). We adopt former value as the distance to X-ray emission.

In this paper, we report X-ray observation of TeV J2032+4130 with Suzaku, which has a higher sensitivity for detecting diffuse X-ray emission with the large effective area and the low stable background. We analyze the diffuse X-ray spectrum of the PWN in detail.

Though Suzaku has the advantage in detecting diffuse X-ray sensitivity, the angular resolution is not sufficient to resolve point sources. To properly estimate the contribution of point sources, we also reanalyze the Chandra data. There are many point sources in and near the Cygnus OB2 region, which are one of the candidate for the origin of TeV emission (e.g., Butt et al. 2006). We resolve point sources within strict parameters, and subtract the point source flux from the diffuse emission. Thus we investigate diffuse emission by combination of Suzaku and Chandra.

## 2. Observations

### 2.1. Suzaku

We observed the TeV J2032+4130 region with Suzaku (Mitsuda et al. 2007) on December 17 and 18, 2007. Suzaku has a moderate angular resolution and a large effective area. This characteristic is suitable for detecting weak diffuse emission. The observations were made using three CCD cameras (X-ray Imaging Spectrometer, XIS; Koyama et al. 2007) on the focal planes of the X-Ray Telescopes (XRT; Serlemitsos et al. 2007). One of the cameras (XIS1) has a back-illuminated (BI) CCD, and the others (XIS0, 3) contain front-illuminated (FI) CCDs. Each of the XIS sensors was operated in the normal clocking mode with the  $5 \times 5$  or  $3 \times 3$  editing mode.

We used clean events processed with the pipeline version of 2.1.6.16. Data taken during the passage through the South Atlantic Anomaly, at elevation angles less than  $5^\circ$  from the night Earth rim, or  $20^\circ$  from the day Earth rim were excluded. After this filtering, the net observing time was about 40 ks.

### 2.2. Chandra

Chandra observed TeV J2032+4130 region twice: an earlier short observation (August 11 2002, obsid=4358)

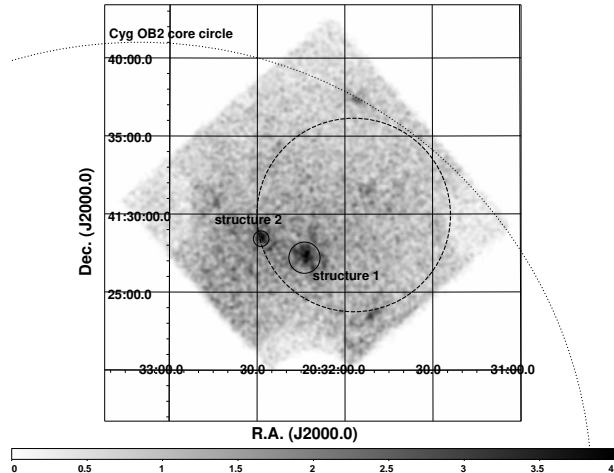


**Fig. 1.** Suzaku image of TeV J2032+4130 (0.5–10.0 keV). Dashed circle indicates the region of diffuse TeV emission. X-ray structures are shown in solid circles. Dotted circle is core circle of Cyg OB2 (Knödlseider 2000).

and a deep follow-up observation (July 19 2004, obsid=4501). The exposure times were 5 ks and  $\sim 49$  ks, respectively. Chandra has a superior angular resolving capability. We analyzed Chandra data in order to estimate the contribution of point sources, using the Chandra Interactive Analysis of Observations (CIAO) software version 4.0.2 with CALDB version 3.4.3. The detailed results about the Chandra observations have already been reported in Butt et al. (2006).

## 3. Results

### 3.1. Images

We first construct a total energy band image of the TeV J2032+4130 region with Suzaku data. Fig. 1 shows an XIS image of 0.5–10.0 keV band. All three CCD data are combined. A dashed circle indicates the TeV diffuse emission region (Aharonian et al. 2005a).

There are two diffuse structures in the circle (structures 1 and 2 in Fig. 1). The extent of X-ray emission is significantly larger than the point spread function. Assuming a Gaussian profile, their sizes are  $\sim 1'.1$  for both structures; however, they are much smaller than the TeV emission.

These X-ray emitting structures are located at the south eastern part of the TeV  $\gamma$ -ray region, and included in the OB star association Cyg OB2 (dotted circle in Fig 1). There must be many point sources in the field. We estimate the contribution of the point sources by the Chandra deep exposure data, which has superior angular resolution, and can resolve weak point sources.

We extracted point sources by the CIAO “wavdetect” software of a wavelet method (Freeman et al. 2002). The threshold significances of wavdetect were set at  $10^{-6}$  for the source list and at 0.001 for the background estimation. The wavelet scales were 1,  $\sqrt{2}$ , 2,  $2\sqrt{2}$ , 4,  $4\sqrt{2}$ , 8,  $8\sqrt{2}$ , and 16 pixels. We then resolved 254 point sources from

the whole region of ACIS-I CCDs. The structure 1 region includes 8 sources, while the structure 2 region includes 2 sources. 158 sources are located in the TeV  $\gamma$ -ray region (dashed circle in Fig. 1), excluding structures 1 and 2.

Fig. 2 shows a Chandra image around structure 1. Point sources are indicated by solid ellipses with the source numbers in Butt et al. (2006). A point source without a number is newly resolved by our analysis. One of the point sources in structure 1, #129, is coincident with the  $\gamma$ -ray pulsar discovered by Fermi (Camilo et al. 2009).

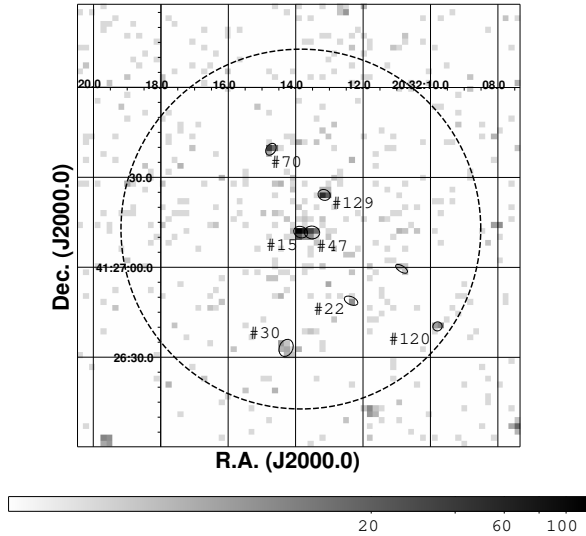


**Fig. 2.** Chandra image of structure 1 (dashed circle). Point sources are indicated by solid ellipses. Labels show the source numbers in Butt et al. (2006). #70 is coincident with #17 in MHG2003, while the combination of #15 and #47 would be #18 in MHG2003 (see also Table 2). A newly detected source has no number. #129 is coincident with the  $\gamma$ -ray pulsar PSR J2032+4127.

### 3.2. Spectra

First, we constructed a spectrum of point sources by Chandra observation in order to estimate the contribution of point sources in the Suzaku image. We collected all the events from the point sources in structure 1, 2 and the remainder of the TeV  $\gamma$ -ray emitting region. X-ray photons are extracted from an ellipse with the axes of  $3\sigma$  of the 2-D Gaussian calculated by *wavdetect* for each source. To reproduce spectra, we fit the spectrum using a phenomenological model of a power-law with an interstellar absorption. The best-fit parameters are shown in “point sources” rows in Table 1.

Then we constructed a spectrum of diffuse emission using Suzaku data. The extracted spectrum of structure 1 is shown in Fig. 3(a). The spectra and responses of three CCDs are combined. We include the contribution of the point sources by adding its best-fit model into the model spectrum, which is indicated by the blue dotted line in Fig. 3(a). Thus, we obtained best-fit parameters

of diffuse X-ray emission for structure 1 (Table 1). The spectrum can be reproduced by an absorbed power-law with a photon index ( $\Gamma$ ) of 2.1, and an absorption column ( $N_H$ ) of  $0.6 \times 10^{22} \text{ cm}^{-2}$ . The X-ray flux is about  $2.0 \times 10^{-13} \text{ erg s}^{-1} \text{ cm}^{-2}$  (2.0–10.0 keV).

We also derived best fit parameters of X-ray spectra extracted from structure 2 and from the remainder in the same manner (Table 1). The best fit models of diffuse and point sources are plotted in Fig. 3(b) and (c). The absorption corrected luminosities (2–10 keV) of diffuse components are  $3.1 \times 10^{32} \text{ erg s}^{-1}$ ,  $3.0 \times 10^{32} \text{ erg s}^{-1}$ , and  $14 \times 10^{32} \text{ erg s}^{-1}$ , for structures 1, 2 and the remaining region, respectively.

In structures 1 and 2, the spectra of point sources are softer than the diffuse component. It indicates that the point source rejection method properly works. It also implies that the origin of diffuse X-ray emission is not a concentration of faint point sources. Most of the point sources in structure 1 and 2 are stars, which generally exhibit softer X-ray emission. The typical temperature of the Cygnus OB2 stars is 1.35 keV (Albacete Colombo et al. 2007). Indeed, the spectra of point sources in structure 1 and 2 can be represented by thin thermal plasma model with the temperature of  $\sim 1 \text{ keV}$ .

### 3.3. Time variation of point sources

We estimated the contribution of point sources using the Chandra data. However, there is uncertainty in the estimated flux because of a possible long term variability of sources. Indeed, Mukherjee, Gotthelf, Halpern (2007) reported a detection of transient X-ray sources in the TeV emission region. We evaluate the uncertainty from the two Chandra observations of TeV J2032+4130 region: an initial 5 ks observation in 2002 (MHG2003) and a deep follow-up exposure of 50 ks in 2004 (But2006). We compared the X-ray count rate of point sources between these two observations.

Earlier observation has poor photon statistics, and detected only 2 sources inside of structure 1. These sources are the #17 and #18 in MHG2003. The follow-up observation detected 7 point sources within the same field as shown in Fig. 2. We made the identification between two observations by the coordinates of these sources. #70 in But2006 is coincident with MHG2003 #17. These sources are identical. While, there are two sources at the position of MHG2003 #18: #15 and #47 in But2006. These sources were too close to resolve in the earlier observation. We consider the count rate of #18 in MHG2003 to be the total of these two sources. Structure 2 only includes identification #14 in MHG2003. This source is coincident with #150 in But2006. We have summarized the count rates of these sources in Table 2.

The count rate of MHG2003 #17 is  $3.0 \times 10^{-3} \text{ counts s}^{-1}$  in 2002, and  $1.5 \times 10^{-3} \text{ counts s}^{-1}$  in 2004. The time variation is  $\sim 2$ . For MHG2003 #18, the count rate is  $7.0 \times 10^{-3} \text{ counts s}^{-1}$  in 2002, which is similar to  $7.2 \times 10^{-3} \text{ counts s}^{-1}$ , the combined count rate of #15 and #47 in Butt et al. (2006).

The count rate of MHG2003 #14 in structure 2 is  $\sim$

**Table 1.** Best-fit parameters of X-ray spectra\*.

		$N_{\text{H}}$ ( $10^{22} \text{ cm}^{-2}$ )	$\Gamma$	$F_{\text{X}}^{\dagger}$ ( $10^{-13} \text{ erg s}^{-1} \text{ cm}^{-2}$ )	$L_{\text{X}}^{\ddagger}$ ( $10^{32} \text{ erg s}^{-1}$ )	$\chi^2$ (d.o.f)
structure 1	point sources	$0.4^{+0.2}_{-0.1}$	$3.1^{+0.5}_{-0.4}$	$0.32^{+0.03}_{-0.02}$		23.0 (14)
	diffuse	$0.6^{+0.4}_{-0.2}$	$2.1^{+0.4}_{-0.3}$	$2.0^{+0.1}_{-0.2}$	3.1	28.6 (31)
structure 2	point sources	$0.4^{+0.8}_{-0.4}$	$3.5^{+2.6}_{-0.9}$	$0.025 \pm 0.006$		0.70 (3)
	diffuse	$0.6^{+0.5}_{-0.3}$	$1.9^{+0.5}_{-0.2}$	$1.9^{+0.3}_{-0.2}$	3.0	1.15 (6)
The remain	point sources	$0.47 \pm 0.07$	$1.8 \pm 0.1$	$9.8^{+0.2}_{-0.3}$		47.1 (23)
	diffuse	$0.7^{+0.2}_{-0.3}$	$2.2^{+0.4}_{-0.3}$	$9.0^{+0.8}_{-0.7}$	14	28.3 (24)

\*: The uncertainties are 90 % confidence level.

$\dagger$ : X-ray flux in the 2–10 keV band

$\ddagger$ : Absorption corrected X-ray luminosity in the 2–10 keV band. The distance is assumed to be 3.6 kpc.

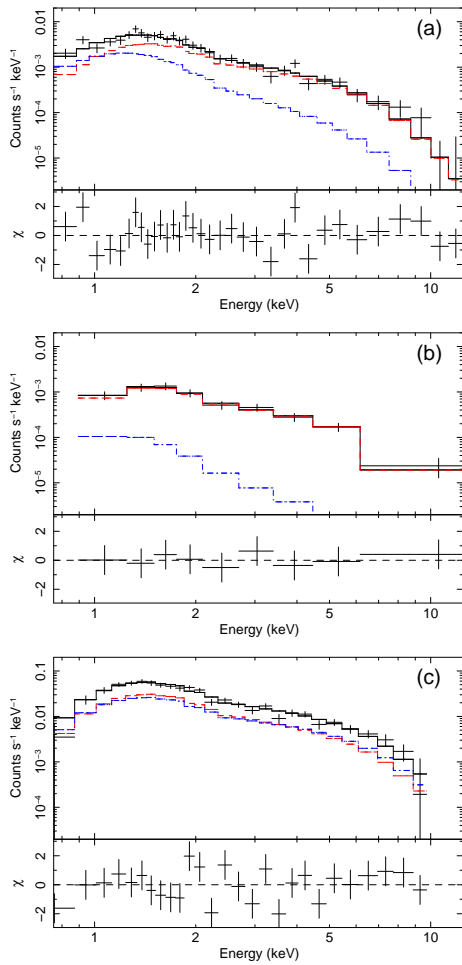


**Fig. 3.** Suzaku spectrum of structure 1, structure 2 and the remaining region of the TeV emission (a, b, and c, respectively). Contribution of point sources is indicated by the blue dotted line in each panel. Red dashed line shows diffuse component.

$4.4 \times 10^{-3} \text{ counts s}^{-1}$  in 2002 and  $0.62 \times 10^{-3} \text{ counts s}^{-1}$  in 2004. The point source indicates the time variability as large as a factor of 7.

As shown in Table 1, the contribution of point sources is about 16.5% and 1.3% for structures 1 and 2, respectively. Even in the largest case of the time variety obtained above (factors 2 and 7), the contribution is about 33% and 9%, respectively. Although these uncertainties of point source fluxes have an influence on the spectrum analysis of diffuse emission, the diffuse emission cannot be explained by the point sources.

#### 4. Discussion

We obtained X-ray spectrum of diffuse emission around the  $\gamma$ -ray pulsar PSR J2032+4127 (structure 1). The photon index is determined to be  $\sim 2$ . This value is coincident with the typical index of X-ray spectrum from PWN:  $\Gamma \simeq 1\text{--}2$  (Kargaltsev & Pavlov 2008). In this section, we consider that the diffuse X-ray emission is radiated by the pulsar wind nebula, and discuss the radiation mechanism.

##### 4.1. Energy injection

First, we discuss the energy injection rate. The spin-down power of the  $\gamma$ -ray pulsar, PSR J2032+4127, is calculated to be about  $2.63 \times 10^{35} \text{ erg s}^{-1}$  (Abdo et al. 2010b). Meanwhile, the isotropic luminosity of the GeV  $\gamma$ -ray pulsar is  $1.4 \times 10^{35} (d/3.6\text{kpc})^2 \text{ erg s}^{-1}$  (Camilo et al. 2009), where  $d$  is the distance to the pulsar. At most about a half of the energy is emitted as GeV  $\gamma$ -rays with an assumption of isotropic radiation. The ratio can be smaller in the case of collimated radiation. The intensity of off-pulse emission is almost the same as background level, which is estimated from surrounding annulus region of the pulsar (Fig. A-42 in Abdo et al. 2010b). Indeed, detailed analysis of off-pulse spectrum cannot constrain the flux level (Ackermann et al. 2011). A large portion of GeV  $\gamma$ -rays originate from the pulsar's magnetosphere, and the luminosity of PWN is negligible in this energy band. Consequently, we cannot obtain meaningful GeV  $\gamma$ -ray flux for PWN. We take no account of the GeV  $\gamma$ -ray band for discussing the energy injection rate from the



**Table 2.** Comparison of X-ray count rate of point sources derived from Chandra data. The time variations of MHG2003 17 and 14 are  $\sim 2$  and  $\sim 7$ , respectively. MHG2003 18 is considered to be a combination of two point sources 15 and 47 in But2006.

	identification		count rate ( $\times 10^{-3}$ count/sec)	
	MHG2003	But2006	2002	2004
structure 1	#17	#70	3.0	1.5
	#18	#15	7.0	4.8
		#47		2.4
structure 2	#14	#150	4.4	0.62

pulsar.

X-ray luminosity and TeV  $\gamma$ -ray luminosity, which are considered to be diffuse emission, are  $\sim 3 \times 10^{32}$  erg s $^{-1}$  and  $\sim 2 \times 10^{33}$  erg s $^{-1}$ , respectively (1.0–10 TeV; Aharonian et al. 2005a, Albert et al. 2008). These are two or three orders of magnitude smaller than the spin-down energy. The spin-down energy is enough to supply X-ray and TeV  $\gamma$ -ray emission. Therefore the energy of the diffuse emission in TeV and X-ray could be supplied by the pulsar, as a PWN. The ratio of  $\sim 10^{-3}$  between X-ray luminosity and the spin-down energy of the pulsar is typical for X-ray emission of PWN (e.g., Figure 10 in Kargaltsev, Pavlov, Wong 2009).

#### 4.2. Emission mechanism

In Fig. 4, we plot the fluxes of X-rays and TeV  $\gamma$ -rays. The X-ray flux is indicated by best-fit model of the diffuse component spectrum of structure 1. The ratio of flux between TeV and the X-ray bands  $F_{\text{TeV}}/F_{\text{X}}$  is  $\sim 10:1$ . Although TeV  $\gamma$ -ray emission dominates the X-ray flux in some PWNe (Funk et al. 2007, Kargaltsev, Pavlov, Wong 2009, Mukherjee, Gotthelf, Halpern 2009), it is difficult to explain such a large ratio with a simple energy distribution of high energy electrons.

If the origin of TeV  $\gamma$ -ray emission is inverse Compton scattering of cosmic microwave background (CMB) by TeV electrons, the same high energy electrons also emit X-rays by synchrotron radiation. In this case, the ratio of TeV flux to the X-ray flux depends only on the magnetic field strength. The synchrotron emission model of TeV electrons are shown by solid lines in Fig. 4 for some assumed magnetic fields of 1, 3, and 10  $\mu$ G. Our data corresponds to the magnetic field of about 1  $\mu$ G. However, this value is much lower than that expected in this region. The total magnetic field strength in the Galaxy disk is larger than 3  $\mu$ G in the whole area (Beck 2001). In addition, active star forming region indicates stronger magnetic field.

If a photon energy density of the local radiation field is much higher than CMB, Compton scattered TeV  $\gamma$ -rays exhibit larger intensity and might explain our data. The number of OB stars are  $\sim 1000$  in Cyg OB2 region. Although we could not rule out the possibility of the strong radiation background, we only consider CMB in this study.

One possibility for resolving the discrepancy is a

hadronic origin of TeV  $\gamma$ -ray emission (e.g., Bednarek & Bartosik 2003). In such a case, X-ray emission can be much lower than leptonic case, and a typical strength of magnetic field of PWNe, 3  $\mu$ G, could be acceptable.

Another possibility is an existence of a high energy cut-off of electrons. The energy of electrons, which is responsible for TeV emission, is lower than X-ray emitting electrons by about one order of magnitude. If the energy distribution of TeV electrons exhibit strong cut-off above the TeV region, the flux of X-ray emission is decreased (dashed line in Fig. 4). Mattana et al. (2009) investigated the evolution of the PWNe by comparing 14 samples, and concluded that the ratio of TeV and X-ray luminosities has a positive correlation with the characteristic age of the pulsar. The X-ray luminosity decreases with the pulsar age because of radiative cooling in the earlier stage (by a factor  $\sim 10^6$  in  $10^5$  yr), while the  $\gamma$ -ray luminosity is constant. Thus, the ratio becomes larger. PSR J2032+4127 is an old pulsar of 120 kyr (Abdo et al. 2010b). The large luminosity ratio might be natural for such an evolved PWN.

This cut-off hypothesis also explains the difference in size between TeV and X-ray emissions as discussed in Aharonian et al. (2005b). X-rays are emitted by young electrons, because higher energy electrons lose their energy quickly. On the other hand, older electrons radiate TeV  $\gamma$ -rays. Such a difference in age could cause the concentration of X-ray emission near the pulsar and the diffusion of TeV emission. Thus the size of X-ray emitting region could be much smaller than that of TeV.

#### 4.3. Other structures

The best-fit parameters of structure 2 are almost the same as structure 1. In addition, the X-ray emission size is also comparable to structure 1. Although no pulsar is found at the location of structure 2, the X-ray emission can be explained by PWN in the same manner as structure 1. If structure 2 is also a PWN, a part of TeV emission could originate from this source.

The remaining diffuse emission also exhibits the same spectral shape as structure 1. However, the X-ray flux and the size is much larger than structure 1, 2. We cannot insist that the remain is related to TeV emission only by the spectral similarities.

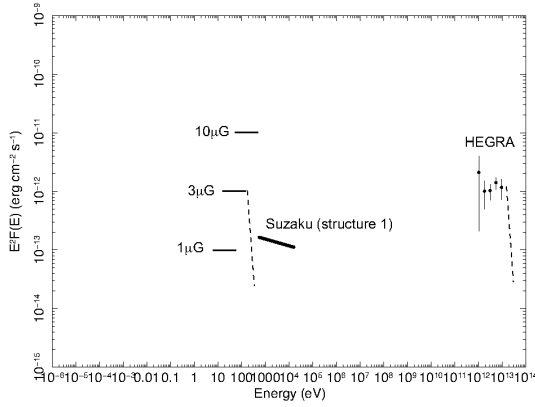


**Fig. 4.** Multiband spectrum of TeV J2032+4130 (TeV: HEGRA spectrum in Aharonian et al. 2005a, X-ray: Best-fit model of the diffuse component of structure 1). Solid lines show synchrotron radiation models with various magnetic field estimated from TeV flux. Dashed line shows an energy cutoff model.

## 5. Summary

We observed the first unidentified TeV  $\gamma$ -ray source TeV J2032+4130 with Suzaku, and detected two structures of diffuse X-ray emission. The position of the structure 1 is coincident with the GeV  $\gamma$ -ray pulsar. We also detected a hint of diffuse emission extended to whole region of TeV emission. By estimating the contribution of point sources by Chandra, we extracted the X-ray spectra of diffuse components. X-ray and TeV  $\gamma$ -ray emission can be explained by electrons with a high energy cut-off above the TeV region, which could originate in old PWN. Such an energy distribution of electrons may lead smaller X-ray emission size in comparison with TeV emission.

This research made use of data obtained from Data ARchives and Transmission System (DARTS), provided by Center for Science-satellite Operation and Data Archives (C-SODA) at ISAS/JAXA.

## References

- Abdo, A. A., et al. 2007, *ApJ*, 664, L91  
 Abdo, A. A., et al. 2009, *Science*, 325, 840  
 Abdo, A. A., et al. 2010a, *ApJS*, 188, 405  
 Abdo, A. A., et al. 2010b, *ApJS*, 187, 460  
 Ackermann, M., et al. 2011, *ApJ*, 726, 35  
 Aharonian, F., et al. 2002, *A&A*, 393, L37  
 Aharonian, F., et al. 2005a, *A&A*, 431, 197  
 Aharonian, F. A., et al. 2005b, *A&A*, 442, L25  
 Albacete Colombo, J. F., Flaccomio, E., Micela, G., Sciortino, S., & Damiani, F. 2007, *A&A*, 464, 211  
 Albert, J., et al. 2008, *ApJ*, 675, L25  
 Beck, R. 2001, *Space Sci. Rev.*, 99, 243  
 Bednarek, W., & Bartosik, M., 2003, *A&A*, 405, 689  
 Butt, Y. M., et al. 2003, *ApJ*, 597, 494  
 Butt, Y. M., Drake, J., Benaglia, P., Combi, J. A., Dame, T., Miniati, F., & Romero, G. E. 2006, *ApJ*, 643, 238 (Butt2006)  
 Camilo, F., et al. 2009, *ApJ*, 705, 1

- Freeman P. E., et al. 2002 *ApJS*, 138, 185  
 Funk, S., Hinton, J. A., Pühlhofer, G., Aharonian, F. A., Hofmann, W., Reimer, O., & Wagner, S. 2007, *ApJ*, 662, 517  
 Gaensler, B. M., & Slane, P. O. 2006, *ARA&A*, 44, 17  
 Hanson, M. M. 2003, *ApJ*, 597, 957  
 Horns, D., Hoffmann, A. I. D., Santangelo, A., Aharonian, F. A., & Rowell, G. P. 2007, *A&A*, 469, L17  
 Kargaltsev, O., & Pavlov, G. G. 2008, 40 Years of Pulsars: Millisecond Pulsars, Magnetars and More, 983, 171  
 Kargaltsev, O., Pavlov, G. G., & Wong, J. A. 2009, *ApJ*, 690, 891  
 Kargaltsev, O., & Pavlov, G. G. 2010, *American Institute of Physics Conference Series*, 1248, 25  
 Knödlseeder, J. 2000, *A&A*, 360, 539  
 Konopelko, A., et al. 2007, *ApJ*, 658, 1062  
 Koyama, K., et al. 2007, *PASJ*, 59, S23  
 Massey, P., & Thompson, A. B. 1991, *AJ*, 101, 1408  
 Mattana, F., et al. 2009, *ApJ*, 694, 12  
 Mitsuda, K., et al. 2007, *PASJ*, 59, S1  
 Mukherjee, R., Halpern, J. P., Gotthelf, E. V., Eracleous, M., & Mirabal, N. 2003 *ApJ*, 589, 487 (MHG2003)  
 Mukherjee, R., Gotthelf, E. V., & Halpern, J. P. 2007 *Ap&SS*, 309, 29  
 Mukherjee, R., Gotthelf, E. V., & Halpern, J. P. 2009, *ApJ*, 691, 1707  
 Serlemitsos, P. J., et al. 2007, *PASJ*, 59, S9